Zero-point spin-fluctuations of single adatoms

Julen Ibañez-Azpiroz,* Manuel dos Santos Dias, Stefan Blügel, and Samir Lounis

Peter Grünberg Institute and Institute for Advanced Simulation, Forschungszentrum Jülich & JARA, D-52425 Jülich, Germany

E-mail: j.azpiroz@fz-juelich.de

Phone: +49 2461 61 8863

Abstract

Stabilizing the magnetic signal of single adatoms is a crucial step towards their successful usage in widespread technological applications such as high-density magnetic data storage devices. The quantum mechanical nature of these tiny objects, however, introduces intrinsic zero-point spin-fluctuations that tend to destabilize the local magnetic moment of interest by dwindling the magnetic anisotropy potential barrier even at absolute zero temperature. Here, we elucidate the origins and quantify the effect of the fundamental ingredients determining the magnitude of the fluctuations, namely the (i) local magnetic moment, (ii) spin-orbit coupling and (iii) electron-hole Stoner excitations. Based on a systematic first-principles study of 3d and 4d adatoms, we demonstrate that the transverse contribution of the fluctuations is comparable in size to the magnetic moment itself, leading to a remarkable $\gtrsim$50% reduction of the magnetic anisotropy energy. Our analysis gives rise to a comprehensible diagram relating the fluctuation magnitude to characteristic features of adatoms, providing practical guidelines for designing magnetically stable nanomagnets with minimal quantum fluctuations.

1

Understanding electron spin dynamics and spin relaxation phenomena of nanomagnets is of capital importance due to both, fundamental motivations and potential technological applications, for instance, in the context of magnetic data storage in the atomic limit. If the hitherto ever-growing trend of magnetic storage density is to be mantained in the future, the magnetic building blocks need to be shrinked to the size of just a handful of atoms. At this scale, however, quantum mechanics pose a serious threat to the stability of the local magnetic moment associated to the nanomagnets, which can be easily perturbed by interactions with their environment.[1–3] In this regard, the stability of the magnetic signal depends crucially on the so-called magnetic anisotropy energy (MAE), an energy barrier generated by the spin-orbit coupling (SOC) that protects and stabilizes the direction of the local magnetic moment against possible fluctuations of the spin, *e.g.* of thermal origin.

Among nanomagnets, single magnetic adatoms represent the smallest possible magnetic unit, thus motivating an intense search for elements that exhibit large and stable magnetic moments when deposited on a substrate. Early theoretical simulations based on density functional theory (DFT)[4–6] boosted this search and created a huge enthusiasm in the field by predicting gigantic local magnetic moments of diverse transition-metal (TM) adatoms, including 4d and 5d elements that are nominally nonmagnetic in bulk. The corresponding experimental scenario, in turn, is notably rich, complex and challenging. On one hand, X-ray magnetic circular dichroism (XMCD) and inelastic scanning tunneling spectroscopy (ISTS) assert that several 3d TM adatoms can possess a substantial MAE of few meV (see *e.g.* refs[7–14]). On the other hand, and in remarkable contrast, the very same adatoms behave as paramagnetic entities when measured by means of spin-polarized scanning tunneling microscopy (SP-STM) (see *e.g.* refs[15–17]), implying the existence of a mechanism that destroys the magnetic stability locally. Going one step further, the case of 4d and 5d adatoms is even more striking, given that they have so far exhibited no clear magnetic signal even when subjected to the static magnetic field of an XMCD experiment, in notorious disagreement with theoretical predictions.[18]

In view of this scenario, a central question arises: what is the mechanism leading to the apparent instability of the magnetic moment of an adatom? In order to address this issue, here we investigate a key dynamical aspect of single adatoms that has not been hithertho considered, namely the contribution of zero-point spin-fluctuations (ZPSF) (see Fig. 1 for a schematic illustration). These are quantum fluctuations present even at absolute zero temperature that can crucially affect the magnetic properties of itinerant electron magnets.[19,20] Here, we elucidate their origin and quantify their impact on the magnetic stability of the series of 3d and 4d TM adatoms deposited on metallic substrates. Remarkably, our first principles investigation reveals that the transverse contribution to the ZPSF is of the order of the local magnetic moment itself, an astonishingly large value that has profound effects on the MAE, which can be reduced by more than 50% with respect to the static value calculated by standard DFT. In order to minimize their destabilizing effect, we pinpoint the three fundamental ingredients that determine the magnitude of the ZPSF, namely the (i) local magnetic moment, (ii) SOC and (iii) electron-hole Stoner excitations. Based on our findings, we develop a simple diagram where the ZPSF of an arbitrary adatom are classified according to the aforementioned factors, offering practical guidelines for stabilizing robust magnetic properties against fluctuations.

The ZPSF are formally given by the fluctuation-dissipation theorem,[21] which relates the variance of the spin-fluctuations, ξ^2, to the imaginary part of the enhanced spin-susceptibility,
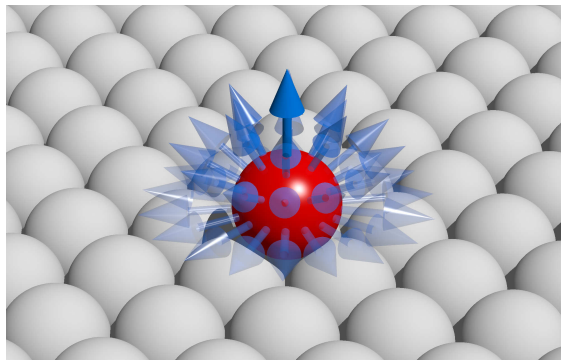

Figure 1: Schematic illustration of the spin-fluctuations (blue arrows) of an adatom (red ball) supported on a surface (grey balls).

Im $\chi(\omega)$. As it turns out, the ZPSF are predominantly determined by the transverse contribution (see Supporting Information), which is given by[21,22]

$$\xi_\perp^2 = -\frac{1}{\pi} \int_0^\infty d\omega \, \text{Im} \, \chi_\perp(\omega). \tag{1}$$

Interestingly, Eq. 1 establishes a deep and insightful connection between the internal fluctuations and the response properties of the system, but its calculation is hard in practice, and no systematic first-principles study of the above quantity has been performed so far.

Let us begin our analysis by discussing Fig. 2, where the calculated spin-excitation and spin-fluctuation spectra associated to TM adatoms deposited on Ag(100) are displayed (see Supporting Information regarding technical details on the formalism and calculations). First, we focus on Figs. 2(a,c), which illustrate the calculated $\text{Im} \, \chi_\perp(\omega)$ for 3d and 4d adatoms, respectively. These figures reveal the existence of a large peak in the meV range for all adatoms, corresponding to a spin-excitation. Noteworthy, the location of the resonance frequency is proportional to the MAE, which in turn is determined by the SOC.[23] Fe shows the largest resonance frequency with $\omega_0 \sim 6$ meV, while for the rest of adatoms we find $\omega_0 \lesssim 4$ meV; in the extreme cases of Ti, V, Mn, Cr and Mo, the spin-excitation is found at very small frequencies, $\omega_0 \lesssim 0.5$ meV, implying that the net effect of SOC is extremely weak in these adatoms. A further feature revealed by Figs. 2(a,c) is the width of the spin-excitation peak, which is linked to the amount of electron-hole Stoner excitations near the Fermi level.[24] Our calculations show that Ru and, to some extent also Nb and Tc, possess large widths as compared to the rest of adatoms, specially those that peak below 1 meV.

Next, we analyze the magnitude of the transverse ZPSF (Eq. 1), as illustrated in Figs. 2(b,d) for 3d and 4d adatoms on Ag(100), respectively; the solid lines depict the evolution of the mean value, $\sqrt{\xi_\perp^2}$, as a function of the upper boundary of the frequency integral, while the converged value is denoted by the horizontal dashed lines (see Supporting Information). The most important message of these figures is that $\sqrt{\xi_\perp^2}$ is of the order of the Bohr magneton;
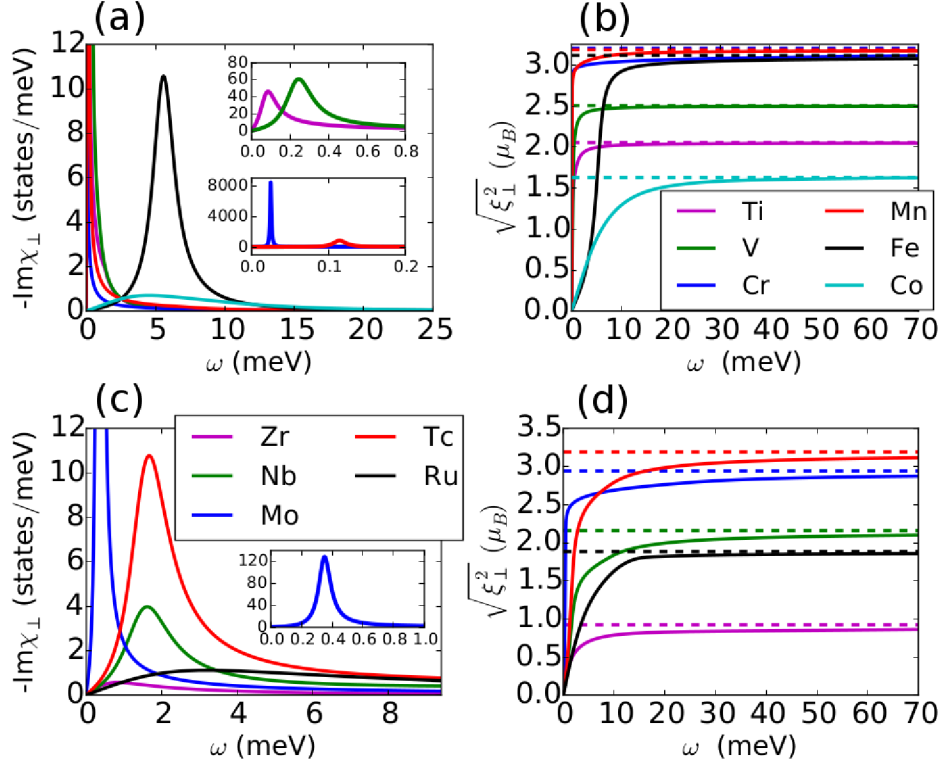
Figure 2: (a) and (c) Density of transverse spin-excitations as given by $\text{Im}\,\chi_\perp(\omega)$ for selected 3d and 4d adatoms on Ag(100), respectively. Insets adress different frequency regions where various resonance frequencies are located. (b) and (d) Calculated magnitude of the mean value of transverse ZPSF for the adatoms considered in (a) and (c), respectively. Solid lines depict the evolution of the value as a function of the upper boundary of the integral of Eq. 1, while the horizontal dashed lines represent the converged value.

the elements with largest values are Cr, Mn, Fe and Tc, which have $\sqrt{\xi_\perp^2} \sim 3\ \mu_B$, while in the case of Zr and Co this value is drastically reduced by more than 50 %. Our calculations further demonstrate that the main contribution to the integral of Eq. 1 comes from the spin-excitation peak in the meV region, which represents between 70 % and $\sim$100 % of the total depending on the adatom.

It is instructive to compare the magnitude of the transverse ZPSF with the local magnetic moments of the adatoms, which we denote as M. This is done in Fig. 3, where it is demonstrated that $\sqrt{\xi_\perp^2}$ (black circles) represents always an appreciable fraction of M (black squares); we find $\sqrt{\xi_\perp^2} \sim M/2$ for Mn and Cr, while $\sqrt{\xi_\perp^2} \sim M$ for Ti, Fe, Zr, Nb and Ru, implying that the latter suffer from very strong deviations of the direction of the local
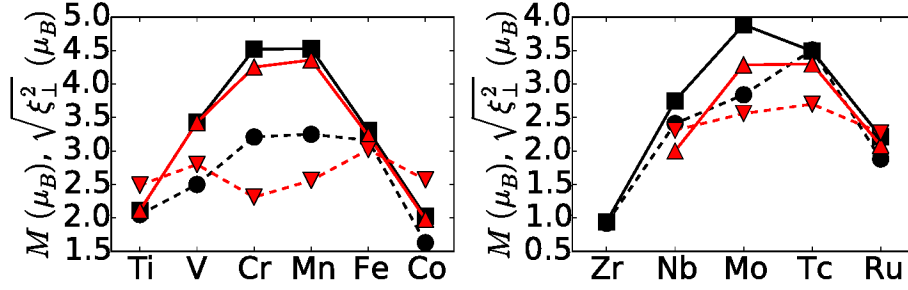
Figure 3: Local magnetic moment (solid lines) and mean value of the transverse ZPSF (dashed lines) for 3d (left pannel) and 4d (right pannel) adatoms. M ($\sqrt{\xi_\perp^2}$) is denoted by black squares (black circles) and red upward triangles (red downward triangles) for adatoms deposited on Ag(100) and Cu(111), respectively.

magnetic moment. It is also noteworthy that both M and $\sqrt{\xi_\perp^2}$ follow the evolution dictated by Hund's rules, whereby the adatoms with nearly half-filled d-shells have largest values: case of Cr and Mn among 3d, and Mo and Tc among 4d. This trend is clearly fulfilled in the case of the magnetic moment, as reported in previous works,[4,5] whereas the evolution of the fluctuation magnitude presents some exceptions, such as the case of Fe and Tc. A further feature revealed by Fig. 3 is that the spin-fluctuation-to-magnetization ratio (SFMR) is overall larger in 4d adatoms than in 3d. As a final remark, we note that Mo has by far the lowest SFMR among 4d elements: interestingly, it is the only 4d adatom deposited on Ag(100) that exhibits an experimentally detectable magnetic signal.[25]

We have extended the above analysis to the same set of adatoms deposited on Cu(111), which exhibit essentially the same features as on Ag(100) (see red triangles in Fig. 3). The only mentionable difference is that the SFMR of Cr and Mn is somewhat lower than what is expected from the trend of Fig. 3; the origin of this feature will be discussed in the next subsection. Our *ab initio* investigation has therefore exposed an important general property of adatoms, namely that the magnitude of their transverse ZPSF is of the order of their local magnetic moment.

We proceed now to identify the fundamental factors that determine the magnitude of the transverse ZPSF. For such purpose, we consider the Landau-Lifshitz-Gilbert (LLG) equation.[26] This is widely employed for characterizing the spin-dynamics of macroscopic magnetic
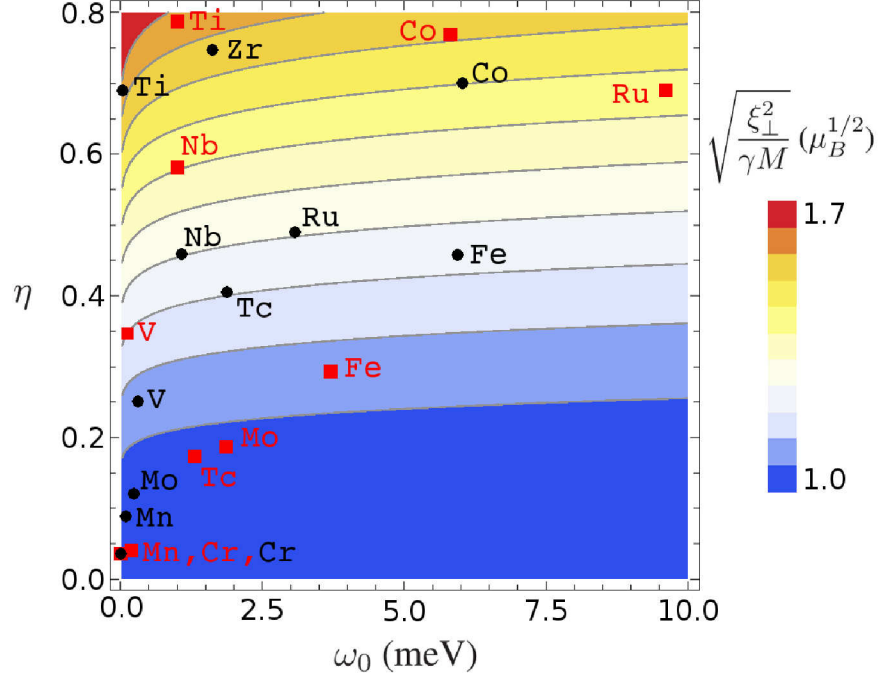
Figure 4: The background shows a 2D plot of the SFMR as a function of the damping and the resonance frequency in the LLG model (Eq. 2). Circles (black) and squares (red) denote various adatoms deposited on Ag(100) and Cu(111), respectively, where the parameters η and ω_0 have been extracted from a fit to the *ab initio* spin-susceptibility.

systems, and its use has been recently legitimated also for microscopic systems,[23,24] as it allows to accurately reproduce the *ab initio* calculations by extracting the relevant parameters. In the LLG model, the imaginary part of the transverse spin-susceptibility takes the form of an skewed Lorentzian, *i.e.* $\mathrm{Im}\chi_{\pm}^{\mathrm{LLG}}(\omega) = C\cdot\eta\omega / \big((\omega-\omega_0)^2 + (\eta\omega_0)^2\big)$, with $C = M\gamma/2(1+\eta^2)$. The parameters entering this model are the Gilbert damping, η, which is proportional to the width of the spin-excitation peak and is therefore dominated by Stoner excitations, and the resonance frequency, $\omega_{\mathrm{res}} = \omega_0\sqrt{1+\eta^2} = \gamma B_{\mathrm{eff}}/\sqrt{1+\eta^2}$, where γ is the gyromagnetic ratio and B_{eff} an effective magnetic field whose magnitude is determined by the strength of SOC; a detailed discussion can be found in, *e.g.*, Ref.[23]

Within the LLG model, the integral of Eq. 1 can be calculated analytically, yielding the following expression for the transverse ZPSF:

$$\xi_{\mathrm{LLG}}^2 = \frac{M\gamma}{\pi(1+\eta^2)}\left(\frac{\eta}{2}\log\frac{(x^2+\eta^{-2}+1)^2 - (2x\eta^{-1})^2}{(\eta^{-2}+1)^2} + \vartheta(x,\eta)\right). \tag{2}$$

Above, $\vartheta(x, \eta) = \arctan(x - \eta^{-1}) - \arctan(x + \eta^{-1}) + 2 \arctan \eta^{-1}$ and $x = \omega_c/\eta\omega_0$, with ω_c a cutoff frequency to be converged (see Supporting Information).

Eq. 2 is very useful as it provides an interpretation for the magnitude of the fluctuations in terms of the physical parameters of the LLG model, which are in turn related to the electronic structure of the adatoms. As anticipated in the introduction, three major ingredients come into play: M, ω_0 and η. Eq. 2 reveals that $\sqrt{\xi_{\text{LLG}}^2}$ is directly proportional to $\sqrt{M}$, which, apart from accounting for the rough proportionality displayed by our calculations (see Fig. 3), it indicates that fluctuations are relatively weaker for adatoms with large magnetic moments, $i.e.$ the nearly half-filled d-shell elements. Interestingly, the simple relationship of Eq. 2 allows to analyze the SFMR, $\sqrt{\xi_{\text{LLG}}^2/\gamma M}$, as a function of η and ω_0 by setting the standard value for the gyromagnetic ratio $\gamma = 2$; the resulting map is displayed in the background of Fig. 4. This figure evidences that the SFMR is critically enhanced by the damping, as $\sqrt{\xi_{\text{LLG}}^2/\gamma M}$ varies by almost 70 % in the range of values considered for η. This feature comes from the fact that enhanced Stoner excitations give rise to a large dissipation of energy, implying large fluctuations via the connection established by the fluctuation-dissipation theorem. It is also noteworthy that when η tends to zero, $\sqrt{\xi_{\text{LLG}}^2/\gamma M} = 1 \; \mu_B^{1/2}$, $i.e.$ Eq. 2 reveals an intrinsic contribution to the transverse ZPSF present even in the limiting case of a spin-excitation with vanishing width. Finally, Fig. 4 demonstrates that the transverse ZPSF are reduced for large resonance frequencies, but, quite unexpectedly, one finds that the induced variation is much less important than with the damping.

We are now in position to perform a quantitative analysis of the $ab\ initio$ transverse ZPSF in terms of the LLG model. For such purpose, we have systematically extracted the parameters η and ω_0 by fitting $\text{Im}\chi_{\pm}^{\text{LLG}}(\omega)$ to the calculated spin-susceptibility ($e.g.$ Figs. 2(a,c)) for all adatoms. This allows us to locate the position of each adatom on the map of Fig. 4, as depicted by the circles and squares for the case of the Cu(111) and Ag(100) substrates, respectively. The resulting distribution makes it clear that the origin of the large
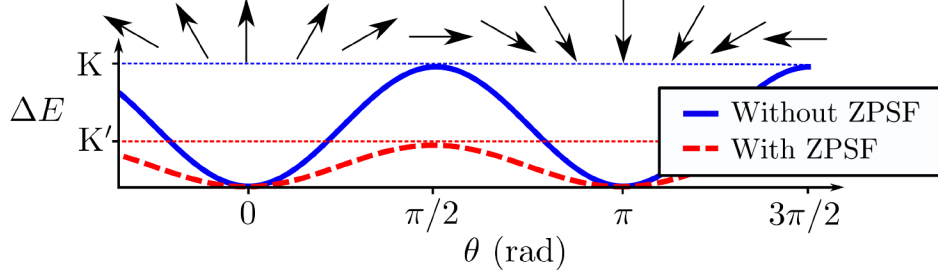
8

Figure 5: Schematic illustration of the renormalization of the MAE induced by the transverse ZPSF. K and K' respectively represent the static and renormalized anisotropy constant (see Eq. 3).

SFMR found in the case of Ti, Co, Ru and Nb on both substrates, as well as Fe and Zr on Ag(100), is mainly due to the large damping factors of these adatoms, $\eta \gtrsim 0.5$, while this tendency is only slightly modified by the position of the resonance frequency. On the opposite side, despite the small resonance frequency of Mn, Cr and Mo adatoms on both substrates, their extremely small damping, $\eta \lesssim 0.05$, makes $\sqrt{\xi_{\text{LLG}}^2/\gamma M}$ approach the intrinsic minimum value.

We note that the distribution of elements shown in Fig. 4 is a guideline to understand the behavior of the SFMR in the context of the LLG model, not an exhaustive representation of the *ab initio* data summarized in Fig. 3. For this reason, some details, such as the larger SFMR of Cr and Mn on Cu(111) than on Ag(100) (see Fig. 3) are not accounted for by the distribution. This particular feature can be attributed to deviations of the gyromagnetic ratio from the standard value $\gamma = 2$, which are larger in the case of Cr and Mn on Cu(111) than on Ag(100)[23] (see Eq. 2).

Having provided an interpretation for the calculated magnitude of the transverse ZPSF in terms of the underlying physical parameters, we come now to analyze its effects on the magnetic stability of the adatoms. For such purpose, we estimate how the fluctuations affect the MAE, as this quantity defines the strength of the magnetic easy axis. We note that the energy scale of the MAE for adatoms is meV,[7,23] which coincides with the energy of spin-excitations that give rise to the primary contribution to the transverse ZPSF (see Fig. 2).

9

Table 1: Calculated anisotropy constants K and K′ for selected 3d and 4d adatoms on Ag(100) and Cu(111).

	Cr	Mn	Fe	Co	Nb	Mo	Tc	Ru
On Ag(100)								
K (meV)	0.22	−0.02	−3.66	−0.46	1.78	1.55	−1.13	−8.32
K′ (meV)	0.05	−0.01	−0.12	−0.08	0.16	0.35	0.01	−0.99
On Cu(111)								
K (meV)	0.21	0.36	−4.73	−3.7	0.55	2.60	3.13	−20.01
K′ (meV)	0.07	0.11	−0.32	1.12	−0.05	0.46	0.44	2.66

Let us consider the expression for the MAE for uniaxial systems, $E_a(\theta) = K(\mathbf{M} \cdot \hat{\mathbf{e}}_z)^2/\mathbf{M}^2 = K \cos^2 \theta$, where K is the so-called anisotropy constant. Consequently, the energy barrier between the magnetic moment pointing along the z axis ($\theta = 0$) and a perpendicular axis ($\theta = \pi/2$) is simply given by $\Delta E = E_a(\theta = 0) - E_a(\theta = \pi/2) = K$, as schematically illustrated in Fig. 5. In the spirit of the spin-fluctuation theory of Moriya,[27] we now let magentic moment to fluctuate around its equilibrium value, i.e. $\mathbf{M}^2 \to (M\hat{\mathbf{e}}_z + \sum_\perp \boldsymbol{\xi}_\perp)^2$. Introducing this term into the definition of $E_a(\theta)$, we obtain a renormalized expression for the MAE, i.e. $E_a(\theta, \xi_\perp^2) = K(M^2 \cos^2 \theta + \xi_\perp^2 \sin^2 \theta)/(M^2 + 2\xi_\perp^2)$. Noteworthy, this implies that the energy barrier gets effectively reduced by the transverse ZPSF,

$$\Delta E(\xi_\perp^2) = K \left(1 - \frac{3\xi_\perp^2}{M^2 + 2\xi_\perp^2} \right) \equiv K', \tag{3}$$

which is characterized by a modified anisotropy constant, K′, as schematically illustrated in Fig. 5.

In Table 1 we have listed the calculated values for both, the anisotropy constant K, which we have evaluated by band energy differences following the magnetic force theorem,[28] and the reduced constant K′, calculated using the values of the magnetic moments and transverse ZPSF of the adatoms. Our calculations reveal a strong and generalized reduction of the MAE, which goes much beyond previous estimates that did not take into account fluctuation effects.[23] For the extreme cases where the ZPSF are larger than M (mostly 4d adatoms), the direction of the local magnetic moment gets completely destabilized, as

reflected by the sign change in the renormalized MAE. It is particularly noteworthy that in the well-studied Fe on Cu(111) system, the ZPSF considerably fix the disagreement between the experimental MAE (~ -1 meV[3,29]) and the theoretical one, which is reduced from K$= -4.73$ meV to K$' = -0.32$ meV. Aside from the numerics, this feature demonstrates that the renormalization of the MAE due to the ZPSF has the correct order of magnitude. Finally, for the 4d TM elements Ru and Nb on Ag(100), where experiments remarkably fail to measure sizable magnetic moments,[18,30] the reduction of the MAE predicted by our calculations is notably large ($\gtrsim 90\%$), indicating that the ZPSF can also play a major role in the absence of stable magnetism observed experimentally.

We have performed a systematic investigation of the impact of transverse ZPSF on the magnetic properties of TM adatoms deposited on metallic substrates. The magnitude of the fluctuations has been accessed via the fluctuation-dissipation theorem, employing the spin-susceptibility of the adatoms calculated *ab initio* within TDDFT. Our analysis has revealed that the transverse ZPSF represent an appreciable fraction of the local magnetic moment of the adatoms, therefore strongly affecting their spin-dynamics. We have identified the nature of the three main ingredients that determine the magnitude of the fluctuations, namely the (*i*) SOC, (*ii*) Stoner excitations and (*iii*) local magnetic moment itself, providing guidance for future search for systems with high stability of the magnetic signal. Additionally, we have shown that spin-fluctuations can strongly reduce the MAE of the adatoms, therefore affecting their magnetic stability and sheding light on the controversies between previous theoretical calculations and experimental observations.

Based on our investigation, we envision that the ideal adatom for technological applications, *i.e.* the magnetically most stable one, should not only posses a large magnetic moment of possibly $4 - 5$ μ_B, but also a large MAE and, above all, a very small damping (*i.e.* virtually no Stoner excitations near the Fermi level) in order to drive the fluctuations to their intrinsic quantum minimum. Within this scenario, the nearly half-filled elements Cr, Mn and Mo emerge as the most promising candidates given that they strongly fulfill the first

and third conditions; however, they exhibit a way too small MAE for real applications when deposited on the Ag(100) and Cu(111) substrates here investigated. The challenge resides therefore in tuning the anisotropy to its maximum value by modifying either the nature of the substrate or the environment of the adatom (*e.g.* nanoislands, surface states, etc.), a subject of intense ongoing investigation (see *e.g.* refs[8,12,31,32]).

The conclusions drawn by the single-adatom case studied in this work settle as a solid background for tackling more complex nanomagnets constituted by several exchange-coupled magnetic adatoms. This playground is particularly attractive given that, contrary to the single-adatom case, several SP-STM experiments have reported an unambiguous observation of stable magnetic moments in this type of composite system (see *e.g.* refs[33,34]), strongly suggesting that local fluctuation effects decrease with increasing cluster size. Interestingly, this feature is in qualitative accordance with one of our main findings in this work, namely that the SFMR associated to the transverse ZPSF becomes smaller the larger the magnetic moment gets. This general trend, however, is likely to be modified by characteristic features associated to clusters, such as the appearance of optical modes in the spin-excitation spectrum (*i.e.* additional peaks in $\text{Im}\,\chi_\perp(\omega)$, see *e.g.* refs[35,36]) that would contribute to the ZPSF as seen from Eq. 1. On top of this, the impact of the ZPSF on the magnetic interactions among different adatoms remains to be fully explored and clarified. We believe that these future steps, alongside with the ones already taken in this work, can crucially contribute to current research efforts for understanding the spin dynamic phenomena of nanomagnets and their stability.

Acknowledgments

References

(1) Hirjibehedin, C. F.; Lin, C.-Y.; Otte, A. F.; Ternes, M.; Lutz, C. P.; Jones, B. A.; Heinrich, A. J. *Science* **2007**, *317*, 1199–1203.

(2) Balashov, T.; Schuh, T.; Takács, A. F.; Ernst, A.; Ostanin, S.; Henk, J.; Mertig, I.; Bruno, P.; Miyamachi, T.; Suga, S.; Wulfhekel, W. *Phys. Rev. Lett.* **2009**, *102*, 257203.

(3) Khajetoorians, A. A.; Lounis, S.; Chilian, B.; Costa, A. T.; Zhou, L.; Mills, D. L.; Wiebe, J.; Wiesendanger, R. *Phys. Rev. Lett.* **2011**, *106*, 037205.

(4) Oswald, A.; Zeller, R.; Dederichs, P. H. *Physical Review Letters* **1986**, *56*, 1419–1422.

(5) Wildberger, K.; Stepanyuk, V. S.; Lang, P.; Zeller, R.; Dederichs, P. H. *Physical Review Letters* **1995**, *75*, 509–512.

(6) Lang, P.; Stepanyuk, V. S.; Wildberger, K.; Zeller, R.; Dederichs, P. H. *Solid State Communications* **1994**, *92*, 755–759.

(7) Gambardella, P.; Rusponi, S.; Veronese, M.; Dhesi, S. S.; Grazioli, C.; Dallmeyer, A.; Cabria, I.; Zeller, R.; Dederichs, P. H.; Kern, K.; Carbone, C.; Brune, H. *Science* **2003**, *300*, 1130–1133.

(8) Rau, I. G. et al. *Science* **2014**, *344*, 988–992.

(9) Honolka, J.; Khajetoorians, A. A.; Sessi, V.; Wehling, T. O.; Stepanow, S.; Mi, J.-L.; Iversen, B. B.; Schlenk, T.; Wiebe, J.; Brookes, N. B.; Lichtenstein, A. I.; Hofmann, P.; Kern, K.; Wiesendanger, R. *Phys. Rev. Lett.* **2012**, *108*, 256811.

(10) Heinrich, A. J.; Gupta, J. A.; Lutz, C. P.; Eigler, D. M. *Science* **2004**, *306*, 466–469.

(11) Hirjibehedin, C. F.; Lutz, C. P.; Heinrich, A. J. *Science* **2006**, *312*, 1021–1024.

(12) Heinrich, B. W.; Braun, L.; Pascual, J. I.; Franke, K. J. *Nano Letters* **2015**, *15*, 4024–4028.

(13) Khajetoorians, A. A.; Schlenk, T.; Schweflinghaus, B.; dos Santos Dias, M.; Steinbrecher, M.; Bouhassoune, M.; Lounis, S.; Wiebe, J.; Wiesendanger, R. *Phys. Rev. Lett.* **2013**, *111*, 157204.

(14) Dubout, Q.; Donati, F.; Wäckerlin, C.; Calleja, F.; Etzkorn, M.; Lehnert, A.; Claude, L.; Gambardella, P.; Brune, H. *Phys. Rev. Lett.* **2015**, *114*, 106807.

(15) Meier, F.; Zhou, L.; Wiebe, J.; Wiesendanger, R. *Science* **2008**, *320*, 82–86.

(16) Khajetoorians, A. A.; Wiebe, J.; Chilian, B.; Lounis, S.; Blügel, S.; Wiesendanger, R. *Nature Physics* **2012**, *8*, 497–503.

(17) Zhou, L.; Wiebe, J.; Lounis, S.; Vedmedenko, E.; Meier, F.; Blügel, S.; Dederichs, P. H.; Wiesendanger, R. *Nature Physics* **2010**, *6*, 187–191.

(18) Honolka, J.; Kuhnke, K.; Vitali, L.; Enders, A.; Kern, K.; Gardonio, S.; Carbone, C.; Krishnakumar, S. R.; Bencok, P.; Stepanow, S.; Gambardella, P. *Physical Review B* **2007**, *76*, 144412.

(19) Aguayo, A.; Mazin, I. I.; Singh, D. J. *Physical Review Letters* **2004**, *92*, 147201.

(20) Ortenzi, L.; Mazin, I. I.; Blaha, P.; Boeri, L. *Physical Review B* **2012**, *86*, 064437.

(21) Callen, H. B.; Welton, T. A. *Phys. Rev.* **1951**, *83*, 34–40.

(22) Giuliani, G. F.; Vignale, G. *Quantum Theory of the Electron Liquid*; Cambridge University Press, 2005.

(23) dos Santos Dias, M.; Schweflinghaus, B.; Blügel, S.; Lounis, S. *Phys. Rev. B* **2015**, *91*, 075405.

(24) Lounis, S.; dos Santos Dias, M.; Schweflinghaus, B. *Phys. Rev. B* **2015**, *91*, 104420.

(25) Beckmann, H.; Schäfer, R.; Li, W.; Bergmann, G. *EPL (Europhysics Letters)* **1996**, *33*, 563.

(26) Gilbert, T. *IEEE Transactions on Magnetics* **2004**, *40*, 3443–3449.

(27) Moriya, T. *Spin Fluctuations in Itinerant Electron Magnetism*; Springer, Berlin, 1985.

(28) Weinert, M.; Watson, R. E.; Davenport, J. W. *Phys. Rev. B* **1985**, *32*, 2115–2119.

(29) Pacchioni, G. E.; Gragnaniello, L.; Donati, F.; Pivetta, M.; Autès, G.; Yazyev, O. V.; Rusponi, S.; Brune, H. *Phys. Rev. B* **2015**, *91*, 235426.

(30) Schafer, R.; Bergmann, G. *Solid State Communications* **1996**, *98*, 45–48.

(31) Ibañez-Azpiroz, J.; Eiguren, A.; Sherman, E. Y.; Bergara, A. *Phys. Rev. Lett.* **2012**, *109*, 156401.

(32) Bryant, B.; Spinelli, A.; Wagenaar, J. J. T.; Gerrits, M.; Otte, A. F. *Phys. Rev. Lett.* **2013**, *111*, 127203.

(33) Loth, S.; Baumann, S.; Lutz, C. P.; Eigler, D. M.; Heinrich, A. J. *Science* **2012**, *335*, 196–199.

(34) Khajetoorians, A. A.; Baxevanis, B.; Hübner, C.; Schlenk, T.; Krause, S.; Wehling, T. O.; Lounis, S.; Lichtenstein, A.; Pfannkuche, D.; Wiebe, J.; Wiesendanger, R. *Science* **2013**, *339*, 55–59.

(35) Lounis, S.; Costa, A. T.; Muniz, R. B.; Mills, D. L. *Physical Review Letters* **2010**, *105*, 187205.

(36) Lounis, S.; Costa, A. T.; Muniz, R. B.; Mills, D. L. *Physical Review B* **2011**, *83*, 035109.